GC
58
.N633
no.17

NOAA Technical Memorandum NOS OES 017

ON THE SPATIAL AND TEMPORAL RESOLVING POWER OF SATELLITE DATA IN REPEAT SAMPLING CONFIGURATION

Silver Spring, Maryland
July 1995

noaa National Oceanic And Atmospheric Administration

U.S. DEPARTMENT OF COMMERCE
National Ocean Service

Office of Ocean and Earth Sciences
National Ocean Service
National Oceanic and Atmospheric Administration
U.S. Department of Commerce

The Office of Ocean and Earth Sciences provides for the understanding of the coastal and ocean environment through the conduct of applied research and development in geophysics; the measurement, analyses, and product development of ocean and lake water levels; the collection, analyses, product development, and disseminations of coastal and global marine data; and the synthesis and interpretation with numerical and mechanistic modeling of global marine data sets. The Office cooperates with the U.S. Navy in conducting oceanographic activities for defense and mixed defense-civil sector purposes and applications.

It plans, develops and coordinates NOAA participation in Federally conducted oceanographic programs and activities, and facilitates cooperative programs, projects and activities with the oceanographic research community. It monitors and analyzes oceanographic activities between NOAA and other organizations and agencies; identifies potential conflicts, overlaps, and opportunities for joint or cooperative efforts; and develops and maintains cooperative agreements, Memoranda of Understanding and other arrangements as appropriate to resolve issues and to ensure maximum benefits from programs of mutual interest. It develops and maintains inventories of oceanographic programs, projects, systems and activities of other organizations and agencies to provide a basis for integrating current and future programs, systems and activities to ensure maximum efficiency and effectiveness in meeting national goals and requirements. The Office conducts research and development; carries out theoretical studies, data analyses, and engineering development; and formulates and executes programs encompassing technological development and application to oceanography, geophysics, geodesy, and related fields.

For the Great Lakes, coastal estuaries, sea coast and oceans, the Office plans, develops, and applies numerical and mechanistic models and produces predictions, forecasts, and analysis guidance materials of oceanographic and related marine meteorological phenomena; collects, analyzes and disseminates tide and water-level observations and associated information; and computes water-level datums for hydrographic, marine boundary and other special surveys. It evaluates and improves methods of data analysis; compares and integrates existing and new classes of data and products; provides and quality controls data sets and an array of output products; and assures science and technology transfer to and from the Office's programs and projects. The Office produces and disseminates operational marine environmental forecast and analysis guidance materials; manages and supports ocean climate studies; installs and operates real-time marine data collection systems; and formulates requirements for marine data sets and for data processing and communications systems; and designs and manages computer-based systems in support of these requirements.

GC
58
N633
no. 17

NOAA Technical Memorandum NOS OES 017

ON THE SPATIAL AND TEMPORAL RESOLVING POWER OF SATELLITE DATA IN REPEAT SAMPLING CONFIGURATION

C. K. Tai

LIBRARY
N.O.A.A.
U.S. Dept. of Commerce

Silver Spring, Maryland
July 1995

United States
Department of Commerce
Ronald Brown, Secretary

National Oceanic and
Atmospheric Administration
James Baker, Under Secretary

National Ocean Service
W. Stanley Wilson
Assistant Administrator

National Oceanic and Atmospheric Administration
TIROS Satellites and Satellite Meteorology

ERRATA NOTICE

One or more conditions of the original document may affect the quality of the image, such as:

Discolored pages
Faded or light ink
Binding intrudes into the text

This has been a co-operative project between the NOAA Central Library and the Climate Database Modernization Program, National Climate Data Center (NCDC). To view the original document contact the NOAA Central Library in Silver Spring, MD at (301) 713-2607 x124 or Library.Reference@noaa.gov.

HOV Services
Imaging Contractor
12200 Kiln Court
Beltsville, MD 20704-1387
January 26, 2009

On the Spatial and Temporal Resolving Power of Satellite Data in Repeat Sampling Configuration

Chang-Kou Tai

NOAA Geosciences Lab.
N/OES11
1305 East-West Highway
Silver Spring, MD 20910

Abstract

The sampling problem for satellite data in exact-repeat orbit configuration is treated here. It is shown there are multitudes of spectral ranges that are resolved with various degree of uncertainty by the data, while the suitable choice depends on the phenomena we wish to observe and the noises we endeavor to avoid. The problem is idealized for applications to regions of limited latitudinal extent so that straight lines represent satellite ground tracks well. Let X and Y be the east-west and north-south separations of parallel tracks, T be the repeat period, and k, *l*, ω be the non-angular wavenumbers and frequency with k in the east-west direction. The spectral range that is perfectly resolved (as if the data were placed on a regular space-time grid) covers (-1/X, 1/X) in k, (-1/Y, 1/Y) in *l*, and [0, 1/2T) in ω. There are other spectral ranges that extend either the spatial or temporal resolution with increased uncertainty beyond the above-mentioned perfectly resolved range.

The idealized problem is solved in stages, progressing from one-dimensional, two-dimensional (2D), to the fully three-dimensional (3D) problem. The process is aided by a discovery that has implications going far beyond the scope of the present paper. It is found that from a multi-dimensional regular grid, we are free to introduce misalignments to all dimensions except one without incurring any penalty in spectral resolution; i.e., the misaligned grid is equivalent to perfectly aligned grid in spectral resolution. (However the misalignment does induce far more complicated aliasing.) Thus non-simultaneous observations are equivalent to simultaneous ones, hence reducing the 3D problem to the 2D one. One 2D grid (the crossover grid) is equivalent to not just one but two regular 2D grids. These results are all verified numerically.

1. Introduction

The peculiar spatial and temporal distribution of satellite observations has presented great difficulties in determining their resolving power, i.e., what maximum range centered on the origin in the frequency-wavenumber space is resolved by the data in the sense that spectral components within the range are sufficiently distinguishable from each other? The resolving power entails a

companion question: What aliasing can be expected from components outside the range into components inside the range? In textbook cases, observations are placed on regular space-time grid such that the Nyquist frequency and wavenumbers are readily determined. In the real world, this is rarely the case. In cases that regular sampling is physically possible, the fiscal constraints often prevent it. Or as in the case of the satellite, the sampling characteristics are constrained by the satellite orbit. Of particular interest is a class of satellites that repeat their ground tracks after a fixed period, thus sampling with a set (albeit irregular) pattern. These include all the altimetric satellites measuring sea level from space. The intelligent choice of a repeat orbit configuration depends on our ability to answer two questions. First, what is the inherent resolving power of a configuration? Second, what are the approximate frequency and wavenumber spectra of the phenomena we wish to observe as well as those of the noises we wish to avoid? The present study will try to answer the former, while discuss the latter only in passing.

There have been two studies on the subject. Wunsch [1989; W89 hereafter] has tried to answer exactly the same question posed here, employing least-squares to explore the resolving power. The least-squares approach can be used to exhaust all possibilities to evaluate the maximum resolving power. However without sufficient theoretical guidance, the cost of an exhaustive search is prohibitive. Thus a slight misunderstanding has rendered W89's results confusing in retrospect. Chelton and Schlax [1994] have taken a different approach by smoothing the irregular data onto a regular space-time grid, then examining the spectral characteristics of the linear smoother (the so-called equivalent transfer function) to determine what range is well resolved after the smoothing operation. But the range clearly depends on the adopted smoother and its associated parameters, while the question posed here is finding the maximum resolving power of a repeat orbit configuration. Here we shall adopt W89's approach, but pepper it with more theoretical development.

The data outage associated with land and data loss can severely complicate the issue and is not treated here. The idealized problem with no data gaps is solved in stages. First, in section 2, the relevant one-dimensional (1D) problem (for either space or time) is shown to be one involving two alternating sampling intervals. The meaning of Nyquist frequency (or wavenumber) undergoes a significant change when data are not equally spaced. Next, we demonstrate in section 3 the important result that observations taken at different times but at regular time intervals (e.g., the exact-repeat sampling by satellites) are equivalent to simultaneous observations, thus simplifying the three-dimensional (3D) problem to a two-dimensional (2D) one. It is shown that of the three dimensions only one needs to be aligned originally. We then solve the idealized 2D problem wherein satellite tracks are straight lines in section 4. The meaning of Nyquist wavenumbers undergoes a even more dramatic change. Finally, in section 5, the idealized 3D problem is solved using the results

obtained for 1D and 2D problems. We conclude in section 6.

2. 1D problem

At crossovers, one has a time series that contains two fixed but alternating sampling periods. Only rarely are the two sampling periods identical (e.g., the 1.5 day at crossovers on the equator for Seasat's 3-day repeat). Similarly along a fixed latitude, one gets a spatial series with alternating sampling intervals. This is also approximately true along a fixed longitude. This recurring 1D problem has significant implications. A thorough understanding is provided here.

a. The damped least-squares approach

W89 gives a complete treatment on spectral analysis of 1D irregularly spaced data. He shows that spectral contents can be obtained through least-squares fitting of Fourier series to the data. Thus the maximum number of unknowns obtainable is the number of data. When data are equally spaced, the maximum range gives the Nyquist frequency. But when data are irregularly spaced, the maximum range may not be obtainable. For example, if two data points are placed too close to each other, they cannot possibly give independent information. In addition, the least-squares solution is more prone to noise (aliasing) with irregularly spaced data. These lead to uncertainties of the least-squares solution that can be handled by the mechanism of the damped least-squares [Hanson and Lawson, 1970; W89 uses the term, tapered least-squares]. If a spectral term's uncertainty (formal error) normalized by the term's signal variance is over 0.5, the term is not resolved at all (see examples in section 2b). This is the basic approach for all our numerical solutions herein. For readers who are uncertain of the details, W89 is a good source.

We solve two cases: one for time series at crossovers, the other for spatial series along fixed latitudes. The difference is in the number of data points. For the former, the number is 147 to model about 2 years (73 repeat cycles) of TOPEX/POSEIDON (T/P), whereas 21 is used to model a east-west span of about 30° in longitudes for T/P. (Note that the number of data points is deliberately kept as odd to avoid the confusion at the highest frequency resulting from unevenly-spaced data.) Of course, one is free to interpret 21 as about 10.5 repeat cycles and 147 as 147 tracks for any satellite. Besides, these disparate numbers provide a hint of how cases may vary according to the total number of data points.

b. Time series with two sampling periods

Thus with 147 data points, we solve for 147 unknowns (Fourier sine and cosine coefficients). The non-angular frequencies are integral multiples of the fundamental frequency, $1/(73.5\times T)$, where T is the repeat period of the satellite (e.g., 10 days for T/P).

The formal error analysis is performed employing the damped least-squares with an a priori noise to signal ratio of 1 (i.e., $\sigma/\Delta=1$, using W89's symbols), but the total noise variance versus the total signal variance is 1 to 74.

The solid line in Fig. 1 displays E, the average normalized uncertainty (i.e., the formal error variance normalized by the signal variance and averaged over the 147 unknowns), as a function of d, the smaller sampling period normalized by the average sampling period, which varies from 0.01 to 1 (where d=1 means the data are equally spaced). It shows very little uncertainty when d=1 to E close to 0.5 (i.e., unresolved) when d is small. The interpretation is straight-forward. When d is extremely small, the data points are bunched together in pairs, essentially only giving 74 independent observations. Thus all spectral terms that would be indistinguishable from each other if we only had 74 equally spaced data become completely confused with each other (as E=0.5 indicates). Between the two extremes, the resolution also lies in between. The individual normalized uncertainties are fairly uniform, thus close to E, the average. The uncertainty also depends on the size of the noise. The dashed line in Fig. 1 shows E versus d if $\sigma/\Delta=2$ (i.e., the error variance is quadrupled).

c. Spatial series with two sampling intervals

In this case, one has 21 data points and 21 unknowns. To keep the total noise variance to total signal ratio at 1 to 74, the a priori noise to signal ratio is changed to 0.39 in the damped least-squares formal error analysis. The dotted line in Fig. 1 shows E versus d. It is barely distinguishable from the solid line except for $d < 0.1$; i.e., the basic conclusions hold even though the number of data points is much reduced.

In summary for sections 2b and 2c, irregular sampling does not allow a clear-cut Nyquist frequency. The maximum spectral range that can be resolved depends on the problem's tolerance for uncertainty and noise. For our particular irregular sampling with two alternating sampling intervals, the maximum resolved frequency (wavenumber) is at least 0.5/(small interval + large interval). Whether it can be doubled to 0.5/(the average interval) is clear for the extremes, yet fuzzy in the transition.

d. Aliasing

The fuzziest issue is aliasing. To get a feel for the problem, here we model a 2-year time series at crossovers for T/P with high-frequency noise at M_2, K_1, S_2, and O_1 tidal frequencies. The noise amplification (i.e., the power of the aliased result divided by the power of the high-frequency noise) is displayed as a function of d for these 4 tidal frequencies in Fig. 2, where it shows the vulnerability to noise is not limited to small d. Note that the noise amplification has been obtained using the damped least-squares with $\sigma/\Delta=1$, without which the results would have been much worse for small d.

It is clear that in the T/P case trying to extend the maximum frequency to 1/(10 days) leaves us vulnerable to noise. But what if we settle for 1/(20 days)? Should not the extra set of observations help reduce aliasing? The answer is yes, but not always. Fig. 3 demonstrates this. Take for example the S_2 tide, whose period is 12 hours. If the time separation between the ascending and descending observations is an integral multiple of 12 hours, there is little reduction in aliasing for S_2. (Note that the exact separations that result in absolutely no reduction can be shown to be close to integral multiples of 12 hours.) But if the separation is 6 hours plus an integral multiple of 12 hours, there is very little aliasing from S_2. In the former case, the two sets of observations are sampling the same S_2 phases, whereas the latter two sets sample phases 180^0 apart. It can be shown for all satellites that the time separation tends to be close to days near the turning latitudes (66^0 for T/P), but close to days plus 12 hours near the equator. The transition from the equator to the turning latitudes is fairly smooth. Thus based on time series at crossovers, S_2 aliasing is more serious in the tropics and near turning latitudes, while K_1 (period 23.93447 hours) aliasing is more prevalent at high latitudes.

3. Equivalency of regular grid and misaligned grid

W89 asserts there is no interesting 2D problem and proceeds directly to the 3D problem. This is the key point that this study departs from W89. Let us take a cue from multi-dimensional Fourier transform, which is done one dimension at a time. Although the observations at different locations are not simultaneous ("asynoptic", according to meteorological usage), the observations at a fixed location are regular in time, allowing easy frequency decomposition at the location. Thus the temporal misalignment has no impact on the 3D Fourier transform in terms of spectral resolution. The same principle applies to the spatial misalignment in one of the remaining spatial dimensions. For example, let us do a 3D transform in x, y, and t. Suppose the data are aligned in x, but not in y and t, even though the sampling is equally spaced in all three dimensions. The transform is done first in t at each fixed x and y. Then we transform in y at each fixed x (which is of course equally spaced). The transform is easily finished in x. In the following, this is verified numerically.

We adopt the following 3D grid: $x=0,1,..,10$, $y=y_0,y_0+1,y_0+2,..,y_0+10$, and $t=t_0,t_0+1,t_0+2,..,t_0+10$, where y_0 and t_0 lie in the interval $[0,1)$,i.e., $0 \le y_0,t_0 < 1$. Note that when $y_0=t_0=0$, it is a regular grid. Now let us keep $y_0=0$, but let t_0 vary with x and y, which is the case of asynoptic observations on a regular spatial grid. To the 3D grid, the following 3D Fourier series is fitted:

$$h(x_m,y_n,t_i) = \sum_{jkl} [c_{jkl}\cos(kx_m/11+ly_n/11-jt_i/11) + s_{jkl}\sin(kx_m/11+ly_n/11-jt_i/11)], \qquad (1)$$

where h represents the data at grid points, while c and s represent the unknowns. The indices vary as follows: m,n,i=0,1,2,..,10 and j=0,1,..,5, while k,l=-5,-4,..,4,5 for j>0, whereas for j=0, k=-5,-4,..,4,5 for *l*=1,2,...,5 and k=0,1,..,5 for *l*=0 with $s_{000}=0$. The interested reader may verify that there are 1331 data points for 1331 unknowns. In (1), we adopt the convention that the frequencies are non-negative, and with the minus sign in front of j, the plain wave propagates in the direction of the wavenumber vector. The damped least-squares error analysis confirms our conjecture. A variety of pattern for t_0 are tried, culminating in a trial with random t_0. Yet all cases yield exactly the same error as the case with $t_0=0$ (i.e., synoptic observations). That is, there is absolutely no penalty on spectral resolution for not having synchronized observations. Furthermore instead of keeping $y_0=0$, we randomize y_0 as well. The result is the same as having $y_0=t_0=0$. We get the same conclusion with a 2D grid. We have not verified this beyond 3D, but it is clear the conclusion should hold for 4D and beyond.

Hence starting from a multi-dimensional regular grid, misalignments (even random ones) along all dimensions except one cause no degradation of resolution; i.e., these misaligned grids resolve exactly the same spectral space as the regular grid. Thus conceptually we can realign grids to make them regular. Most of the spatial grids to be considered in the next section is either regular or misaligned regular. But even if the spatial grid is not regular or misaligned regular, the 3D problem is reduced to a 2D one by the 3D Fourier transform argument.

However the misalignment does induce much more complicated aliasing than the straight-forward case with the regular grid. The aliasing depends on the exact nature of misalignment, thus has to be handled in a case-to-case basis. This is beyond the scope of the present paper.

4. Idealized 2D problem

a. Idealized ground tracks

Fig. 4 plots an idealized track configuration with two sets of equally spaced parallel straight lines, which intersect to form identical diamonds. The configuration is completely specified with two numbers: the east-west separation between the two corners of the diamond (called X), and the north-south separation of the other two corners (called Y). Note that X, Y are simply the east-west and north-south separations between adjacent parallel tracks. For regions with limited north-south extent, the idealized tracks approximate well the real tracks on a latitude-longitude plot. As the center of the region moves latitudinally, X in longitude remains the same, while Y in latitude changes with the appropriate regional idealization. Take T/P for example, Y is slightly less than 3X around the equator, Y=2X around 28^0 latitude, Y=X near 47^0, then Y shrinks fast with Y=X/2 near 57^0, Y=X/3 near 61^0, Y=X/4 near

63^0, and Y=X/5 near 64^0, etc. In terms of distance, X changes with latitude too. X equals 2.835^0 longitude for T/P, 1.475^0 for Geosat 17-day repeat, 0.719^0 for ERS-1 35-day repeat, and 8.372^0 for Seasat 3-day repeat.

It should be noted that for regions with substantial north-south extent, the Fourier harmonic analysis (to which we have restricted ourselves in this study) is no longer valid. Analysis should be based on spherical harmonics, and land cannot be ignored.

b. Along-track wavenumber spectra

The idealized tracks show two directions that are richly sampled. Fu [1983] and Le Traon et al. [1990] have produced along-track wavenumber spectra, taking advantage of the dense along-track sampling. Suppose s is the meaningful along-track sampling interval, S is the shortest distance between parallel tracks. Note that $S > s$. Then from the ascending tracks alone, the resolved spectral range on the k*l* wavenumber plane (where k and *l* are non-angular wavenumbers being positive in the east and north direction respectively) is an elongated rectangle in the direction of the ascending tracks and passing though the origin at its halfway point with a length of 1/s and a width of 1/S. The descending tracks lead to a corresponding rectangle in the direction of the descending tracks. They overlap in a diamond (the same shape as those in Fig.4) around the origin. Note that in this study, we adopt the convention that k and *l* can be positive or negative, but the frequency, ω, is always non-negative. This oddly x-shaped region on the k*l* plane represents the spectral region that is resolved by the data except in the vicinity of the origin, where the overlap complicates the issue.

c. What is a meaningful 2D spectral range?

The x-shaped region, besides stating high-resolution along-track spectra can be produced, is not meaningful for 2D data analysis. A meaningful range should have comparable resolution in all direction. That is, the meaningful range lies in the region where the overlap occurs. Recall the ambiguity with the resolved spectral range for 1D irregularly spaced data. Now we have the additional problem concerning the shape of the range in 2D. Is it a rectangle on the k*l* plane with its sides parallel to the k and *l* axes (i.e., independent ranges in k and *l*)? This conforms to our usual notion and, in fact, will be the shape adopted here. But in general it does not have to be a rectangle. Even if it is a rectangle, it does not have to be oriented this way. (It happens that for data distribution depicted in Fig. 4, this orientation is right.) It will become clear that even for our adopted shape, there is arbitrariness, which can only be removed by other considerations. In fact, there is so much ambiguity in the resolved spectral range that even if our adopted rectangular shape is not exactly right, it serves the purpose.

In the following, we show various resolved ranges based on

various subsets of data points marked in Fig. 4. All ranges are appropriate under the right circumstances, depending on one's desire for larger spectral range or less noise amplification.

d. 2D ranges resolved by the crossovers: the crossover grid

The crossovers are special because they may have temporal resolution up to 1/T or at least have less aliasing if resolution up to 1/2T is sought (see sections 2b and 2d). These points form two independent regular grids with sampling intervals of X and Y (those marked by ▵ and those by ▿ in Fig. 4), each resolving the same spectral range, (-1/2X,1/2X) in k and (-1/2Y,1/2Y) in *l*, with an area of 1/XY. This is the problem of "non-simultaneous" observations in x and y. We can realign (see section 3) from the ▵ grid locations to those aligned with the ▿ grid.

There are two ways to accomplish this, resulting in two different regular grids. From ▵'s along fixed y's, one can realign them to x's that are aligned with ▿'s. Denoting these by ▲ on Fig. 4, we see that these and ▿'s form a regular grid with intervals of X and Y/2, resolving the range, (-1/2X,1/2X) in k and (-/Y,1/Y) in *l*, with an area of 2/XY. On the other hand, one can also realign ▵'s along fixed x's to y's aligned with ▿'s. Denoting these by ▼ on Fig. 4, then they and ▿'s form a grid with intervals X/2 and Y, resolving the range, (-1/X,1/X) in k and (-1/2Y,1/2Y) in *l*, also with an area of 2/XY. Numerical verification with the crossover points using these two spectral ranges shows that each range results in the perfect resolution as if the crossovers were located on a regular grid.

Thus one has the ultimate in ambiguity that the same data points actually support two equally well resolved ranges. If we want to keep resolution in k and *l* as close as possible, the former is preferred in the tropics and mid-latitudes, while the latter is for high latitudes. As if this is not confusing enough, one may pose the question: Is any rectangular range, $(-1/L_x,1/L_x)$ in k and $(-1/L_y,1/L_y)$ in *l*, with $L_xL_y=2XY$ while $L_x\leq 2X$ and $L_y\leq 2Y$, equally well resolved? Numerical verification shows that while the two ranges produced by realignment give as perfect a resolution as a regular grid, any other ranges cause degradation. As stated in section 3, it is really the realignment that works here.

e. The 2D range resolved by mid-points between crossover points: the mid-point grid

These points (which are called the mid-points hereafter) are marked by ● on Fig. 4, where they form a regular grid with intervals of X/2 and Y/2, resolving the range, (-1/X,1/X) in k and (-1/Y,1/Y) in *l*, with an area of 4/XY. The mid-point grid gives twice the spatial resolution than the crossover grid.

f. 2D ranges resolved by points midway between crossover points and mid-points: the quarter-point grid

This represents an attempt to extend the resolution in one (but not both) direction at the cost of more uncertainty. The points (which are called quarter-points hereafter) are marked by o in Fig. 4, which are obviously not on a regular grid. Nor can they be realigned onto a regular grid. However we can do the 2D Fourier decomposition one dimension at a time as well. This can be done in two ways. First, for spatial series along fixed y's, the two sampling intervals are X/4 and 3X/4, from which 1D Fourier series can be obtained as described in section 2. From Fig. 1, the uncertainty is reasonably small (for d=0.5) for these 1D Fourier series with resolution of (-1/X,1/X) in k. These series are available along y's that are Y/4 apart. Thus further transform in y resolves the range (-2/Y,2/Y) in *l*, resulting in an resolved spectral area of 8/XY, which is twice the spatial resolution of the mid-points, but at the cost of more uncertainty. Second, following the same logic but switching the roles of x and y resolves the range, (-2/X,2/X) in k and (-1/Y,1/Y) in *l*, also with an area of 8/XY. As in section 4d, which is preferred depends on which direction we want more resolution.

The damped least-squares error analysis is performed to verify these conjectures. A nondimensionalized grid corresponding to Fig. 4 is used with one set of crossovers at x,y=0,1,2,..,10 and another set of crossovers at x,y=0.5,1.5,2.5,..,9.5. The mid-points are at midway between the crossovers, while the quarter-points are midway between mid-points and crossovers. To this grid, a 2D Fourier series is fitted:

$$h(x,y) = \sum_{kl} [c_{kl}\cos(kx/11+ly/11)+s_{kl}\sin(kx/11+ly/11], \qquad (2)$$

where h,c,s are as defined in (1), *l*=0,1,2,..,L, whereas k=-K,-K+1,-K+2,..,K-1,K for *l*>0 and k=0,1,..,K-1,K for *l*=0 with $s_{00}=0$. The interested reader may verify that there are 1421 data points and (2K+1)×(2L+1) unknowns.

The mid-points form a 20x20 regular grid. Thus the spectral range with K=L=9 represents the well-resolved range by the mid-points. The upper panel of Fig.5 shows the normalized uncertainty in percent for this range using $\sigma/\Delta=1$ in the damped least-squares. This range is indeed well resolved with the average uncertainty of 0.86% and no uncertainty greater than 1.25%. As discussed previously, the quarter-points are equivalent to a 20x40 or a 40x20 regular grid with increased uncertainty. The middle panel of Fig. 5 shows the normalized uncertainty for the corresponding range with K=9 L=19. (One can get the equivalent result with K=19 L=9.) As anticipated, the average normalized uncertainty increases to 4.39% with the highest at 8.62%. In addition, the vulnerability to noise amplification could be much worse as demonstrated in section 2d. To illustrate once more the importance of our interpretation of Fourier transform with one dimension at a time, the bottom panel of Fig. 5 shows the uncertainty for the range K=L=13. Note the number of unknown sought in this case is 729 (i.e., less than the 741

unknowns sought in the case with K=19 L=9). Yet the average uncertainty has increased to 8.54%. And more importantly the largest uncertainty is over 30%, spreading over significant portions of the range and signaling the range is not well-resolved at all.

We can extend the logic to get fairly high resolution along one of the direction if the problem demands it and can tolerate the increased uncertainty.

g. Along-track low-pass filtering to reduce the aliasing

One may pose the question: What happens to all the unmarked data points? Aren't they wasted? The answer is no. Sections 4d,4e and 4f more or less show the maximum resolving power of the 2D data set, while smaller scales cause aliasing, which is where the rest of the data contribute. Along-track low-pass filtering reduce not only spatial aliasing but also temporal aliasing from high-frequency small-scale phenomena, e.g., instrumental noise, etc. The notable exceptions are the so-called basin modes and the tide error. The simplest filtering can be achieved by combining the along-track data partitioned evenly surrounding points with the same mark. For example, we get the mid-point data by averaging data between crossovers.

5. Idealized 3D problem

Now we are in a position to answer the question posed in the introduction by combining the results of the preceding three sections. As in the 2D case, there are a multitude of resolved ranges, each appropriate under the right circumstance. These are discussed one by one in the following. We have restricted ourselves to rectangular ranges in 2D. Here in 3D, we shall restrict the shape to that of a cuboid (see section 4c for elaboration; also note that if the three sides of a cuboid are equal, it becomes a cube). However it is too optimistic to expect no new complications to result from the additional dimension. This produces some speculations on additional resolved ranges with high temporal but low spatial resolution.

a. 3D spectral ranges resolved by the crossover grid

If one is content with temporal resolution up to 1/2T with less temporal aliasing, the data resolve two 3D ranges with the 2D ranges in section 4d complemented by the ω range of [0,1/2T), resulting in 3D spectral volume of 1/XYT with no increase in uncertainty than regular grids. If, on the other hand, temporal resolution up to 1/T is sought, the uncertainty is certainly increased (see sections 2b and 2d). The question is by how much. Here we compute the uncertainty numerically for two T/P cases.

We adopt the following non-dimensional grid: x=0,1,2,..,10 y=0,1,2,..,4 for one set of crossovers, and x=0.5,1.5,2.5,..,10.5 y=0.5,1.5,2.5,..,4.5 for the other set. At each crossover, $t=t_0$,

t_0+1, t_0+2,.., t_0+6 where $|t_0|<1$ is the ascending or descending time in the beginning cycle (seven repeat cycles are used here). For a pair of parallel tracks, the eastern one is sampled three days later than the western one. Thus to specify the temporal sampling, all we have to do is to specify the ascending and descending times for one crossover point, say the point x=y=0. Two cases are examined with y=0 corresponding to 2^0N and 43^0N respectively.

To this grid, the Fourier series specified by (1) is fitted. From section 4d, we know the spatial grid is equivalent to a 11x10 regular grid. Thus we choose K=5 L=4. If we are content with resolution up to 1/2T (i.e., with J=3), the damped least-squares error analysis yields for both latitudes the same result as if the spatial grid were a regular 11x10 grid and the temporal sampling were synchronized. With $\sigma/\Delta=3$, the uncertainty is 0.58% for j=k=l=0 and 1.16% for the rest. Now let us extend the resolution to 1/T (i.e., with J=6). The results are shown in Fig. 6. The top panel displays the uncertainty for j=0 for both cases, where it shows the uncertainty of the temporal mean for both cases when J=6 remains the same as when J=3. For j>0, the uncertainty varies only slightly with different j and is indistinguishable as displayed. Thus only one uncertainty plot is shown for j=1,2,..,6. The middle panel shows the uncertainty for j>0 of the 2^0N case, whereas the bottom panel shows the corresponding 43^0N case. The uncertainty is indeed heightened, though not as bad as anticipated. The vulnerability to noise amplification could be much worse though (see section 2d).

b. 3D Range resolved by mid-point grid

The 2D range described in section 4e is supplemented by [0,1/2T) in ω, totaling 2/XYT in volume. This range gives the largest resolved spectral space with no increase in uncertainty than a regular grid.

c. 3D ranges resolved by quarter-point grid

Complementing [0,1/2T) in ω to the 2D ranges depicted in section 4f, we get two 3D ranges, each with resolved spectral space of 4/XYT, i.e., twice as large as the mid-point range, but at the cost of increased uncertainty.

d. 3D ranges with high temporal but low spatial resolution

The following heuristic example shows that we can sacrifice spatial resolution to gain more temporal resolution. In the extreme case, if only the spatial mean is sought, then (ignoring aliasing for the moment) the mean is observed every second except when the satellite is over land. It is a resolved range in the sense that no two components in the range are confused with each other. Yet the choice is obviously not sensible. This narrowest spatial range makes noise out of all other spatial scales, entailing the need for severe smoothing. We can get a reasonable estimate for the mean only by averaging data that are more or less evenly distributed

over the globe. An entire repeat cycle is a good choice, but then we end up with no better temporal resolution than any of the cases considered so far. The compromise is one day.

The one-day tracks more or less cover the whole globe, but they do not repeat themselves every day. The biggest longitudinal excursion from the first one-day tracks in each repeat cycle is 14.17^0 for T/P, 11.80^0 for Geosat 17-day repeat, and 12.22^0 for ERS-1 35-day repeat. If we are content with resolving spatial scales much larger than these excursions, the fact that the patterns do not repeat exactly becomes less important. Note that the so-called exact repeat only means repeating within 1 km of the nominal track at the Equator.

Satellites have near-repeat sub-cycles. For example, T/P, Geosat 17-day repeat, and ERS-1 35-day repeat all nearly repeat every 3 days; i.e., in 3 days, an evenly distributed ground track pattern is produced, then the whole pattern is shifted to the east (west) by 2.835^0 or 1.475^0 (1.437^0) longitude in the following 3 days for T/P or Geosat (ERS-1). In addition, ERS-1 has a 16-day near-repeat sub-cycle, wherein the 16-day pattern is shifted to the east by 0.719^0 longitude in the following 16 days. However, these near-repeat sub-cycles drift off continuously in one direction, causing the biggest excursion of the patterns to be no better than the one-day pattern.

These high temporal but low spatial resolution resolved spectral ranges may be useful for analyzing barotropic Rossby waves and gravity waves of basin scales, as well as large-scale environmental correction errors, e.g., atmospheric pressure related corrections and ionospheric correction. We have not verified these conjectures numerically. Thus these are better viewed as speculations for now, to be proved or disproved later.

6. Discussion

W89 fits 17 days of Geosat or T/P sampling (real or simulated) in the North Atlantic ($32\text{-}46^0$N, $280\text{-}315^0$E) with a Fourier series in the 3D range: ($-1/6^0$, $1/6^0$) in k and *l*, [0, 1/(4.25 days)) in ω. In retrospect, the sampling is clearly not capable of resolving this high-frequency range as confirmed by his results. As discussed in section 5d, in order to get temporal resolution that high, the spatial resolution has to be sacrificed. In any rate, it is not the special high-frequency range that is the most meaningful; Rather, it is the ranges described in sections 5a, 5b and 5c that have the maximum resolved spectral space. Chelton and Schlax [1994] concludes that the Geosat orbit configuration is capable of resolving scales of about 3^0 in latitude and longitude by about 30 days. Considering that Y is about 3^0 in mid-latitudes and X is 1.475^0 and T is 17 days, they come fairly close, albeit still missing the perfectly resolved range (the mid-point grid) by a factor of 2.

The problem is by no means solved. The aliasing for a specific satellite and specific grid is yet to be determined. The impact of missing data, land, or large latitudinal extent is not yet clear.

We still have to determine the 3D spectrum of the sea level and noise, then what satellite sampling configuration is the most advantageous.

Acknowledgment John Kuhn did the plotting. The work was supported in part under NASA's TOPEX Altimetry Research in Ocean Circulation Program and in part by the NOAA Climate and Global Change Program.

References

Chelton, D. B., and M. G. Schlax, The resolution capability of an irregularly sampled dataset: with application to Geosat altimeter data, *J. Atmos. Oceanic Tech.*, *11*, 534-550, 1994.

Fu, L.-L., On the wavenumber spectrum of oceanic mesoscale variability observed by the Seasat altimeter, *J. Geophys. Res.*, *88*, 4331-4341, 1983.

Le Traon, P. Y., M. C. Rouquet, and C. Boissier, Spatial scales of mesoscale variability in the North Atlantic as deduced from Geosat data, *J. Geophys. Res.*, *95*, 20267-20285, 1990.

Wunsch, C., Sampling characteristics of satellite orbits, *J. Atmos. Oceanic Tech.*, *6*, 891-907, 1989.

Figure Legends

Fig. 1 Results of the damped least-squares formal error analysis for fitting Fourier series to time (or space) series having two alternating sampling intervals. E equaling 0.5 or higher indicates the average spectral term is completely unresolved. The solid (dashed) line is for the case with 147 data points and a priori noise to signal ratio of 1 (2), while the dotted line is for the case with 21 data points and ratio of 0.39. See sections 2b and 2c.

Fig. 2 Fitting time series of 147 data points with the Fourier series with 147 unknowns at TOPEX/POSEIDON (T/P) crossovers [i.e., trying to resolve up to 1/(10 days)], the noise at M_2 (solid), K_1 (dashed), S_2 (dotted), O_1 (chain dashed) tidal frequencies is not only aliased but amplified. See section 2d.

Fig. 3 Same as Fig. 2 except the Fourier series has 73 unknowns [i.e., trying to resolve only up to 1/(20 days)]. Not only is there no noise amplification, but the aliasing is reduced in many cases. See section 2d.

Fig. 4 The idealized satellite ground tracks. The crossover grid is represented by points marked with Δ or ∇ (section 4d, which shows these points can be realigned into two regular grids). The mid-point grid is represented by points marked with $\bullet$, which form a regular grid already (section 4e). The quarter-point grid is represented by points marked by o, which can not be realigned into any regular grid, but nonetheless can undergo 2D fourier analysis (section 4f).

Fig. 5 Top panel: The normalized uncertainty, (error variance)/(signal variance) in percent, in the well resolved spectral range by the mid-point grid. Middle panel: The normalized uncertainty in the extended spectral range (the resolution in y is doubled in this case) by the quarter-point grid. Or equivalently the resolution in x can be doubled. Bottom panel: The normalized uncertainty in a range with extended resolutions in both directions. Even though less unknowns are sought with this range, the uncertainty is greatly increased. See section 4f.

Fig. 6 The normalized uncertainty, (error variance)/(signal variance) in percent, in the 3D spectral range resolved by the crossover grid. Top panel: $\omega=0$ (i.e., the mean) which is the same for two simulated T/P crossover grids with the southernmost latitude at 2°N or 43°N. Middle panel: $\omega\neq0$ for the simulated T/P crossover grid with its southernmost latitude at 2°N. Bottom panel: $\omega\neq0$ for the simulated T/P crossover grid with its southernmost latitude at 43°N. The uncertainties for non-zero frequencies only differ slightly and would be indistinguishable if shown. See section 5a.

Fig. 1

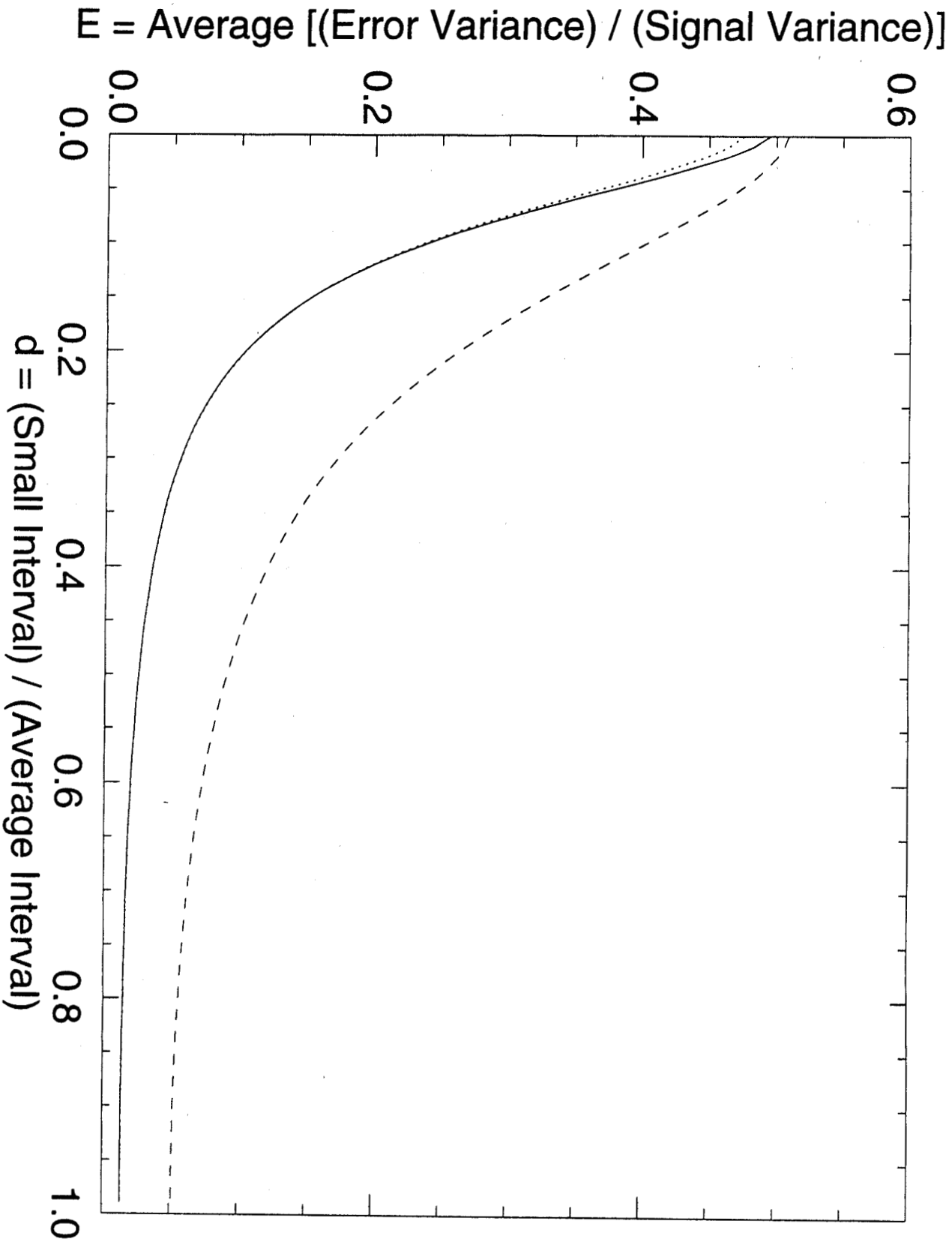
E = Average [(Error Variance) / (Signal Variance)]
0.0
0.2
0.4
0.6
0.0
0.2
0.4
0.6
0.8
1.0
d = (Small Interval) / (Average Interval)

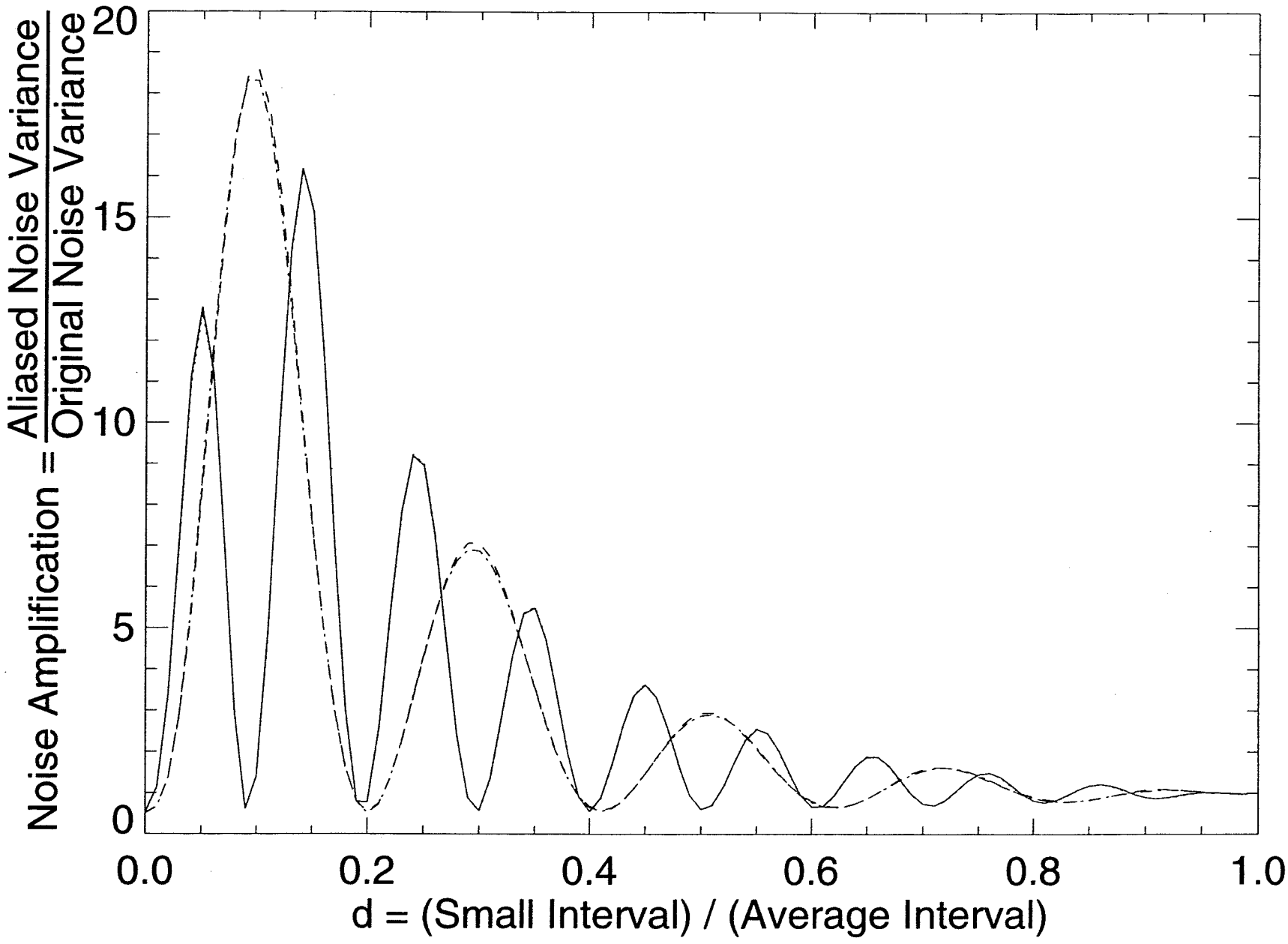
Noise Amplification = Aliased Noise Variance / Original Noise Variance
20
15
10
5
0
0.0
0.2
0.4
0.6
0.8
1.0
d = (Small Interval) / (Average Interval)

Fig. 2

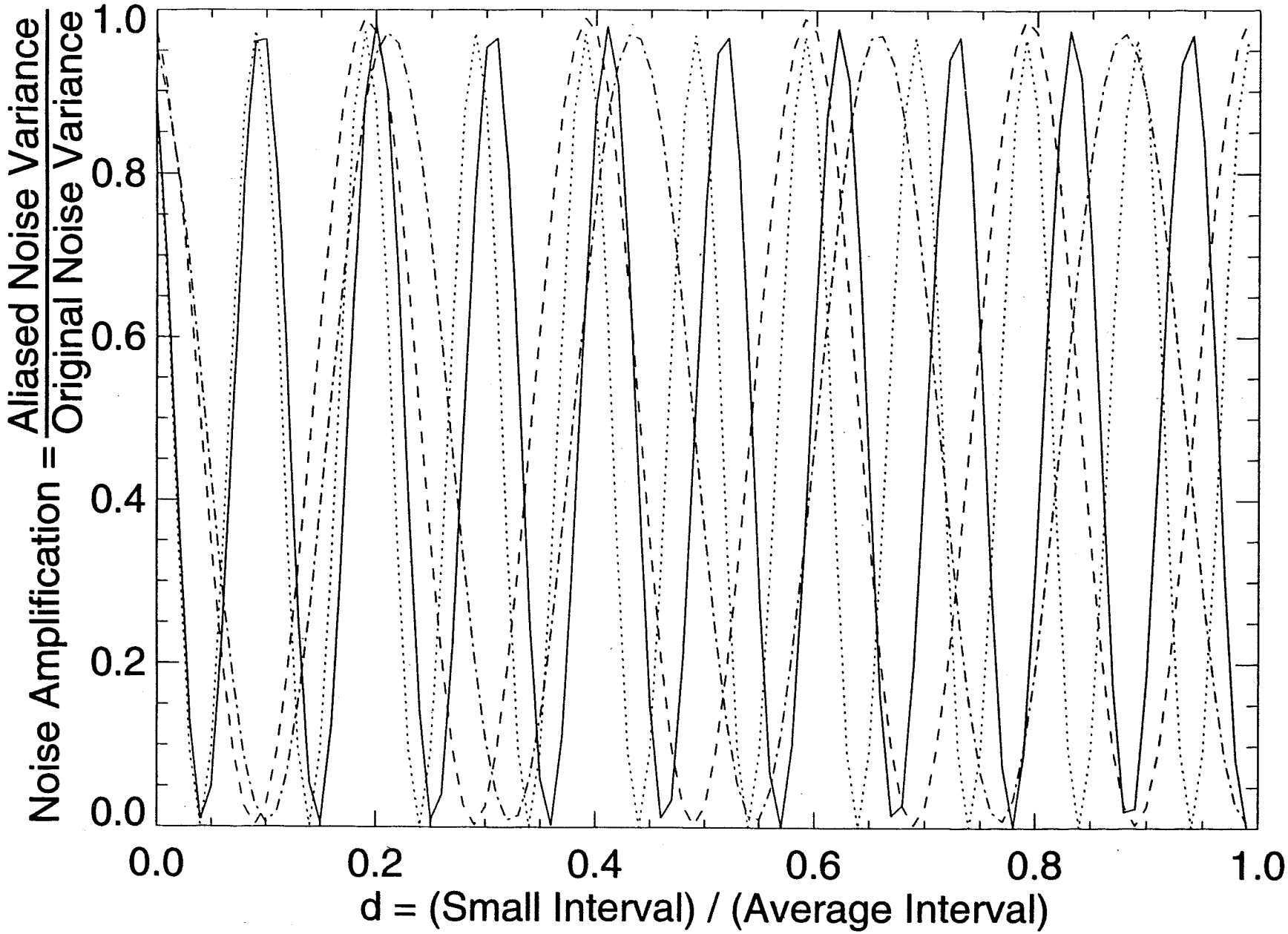
Noise Amplification = Aliased Noise Variance / Original Noise Variance
1.0
0.8
0.6
0.4
0.2
0.0
0.0
0.2
0.4
0.6
0.8
1.0
d = (Small Interval) / (Average Interval)

Fig. 3

Fig. 4

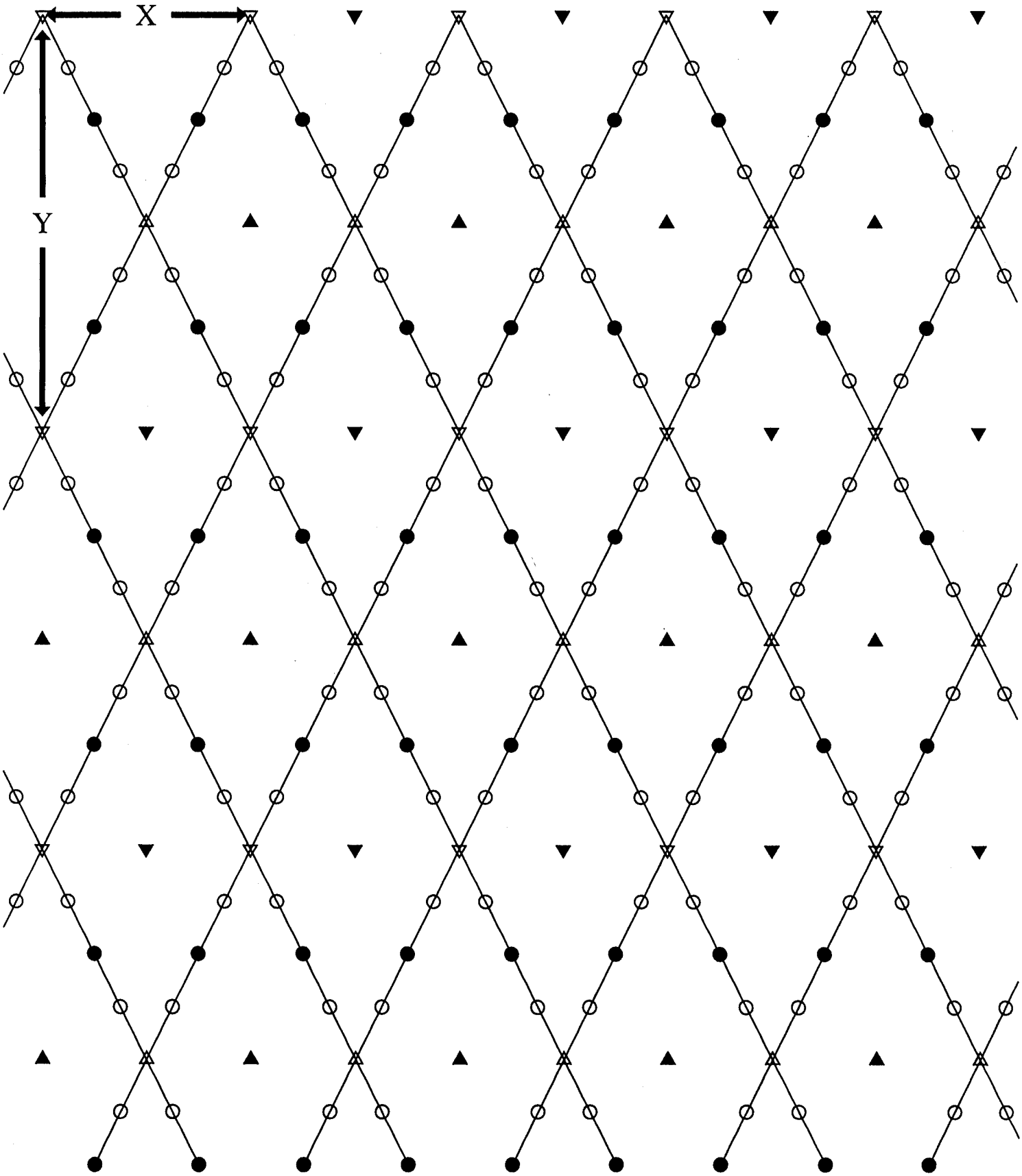

Fig. 5

Percentage Uncertainty

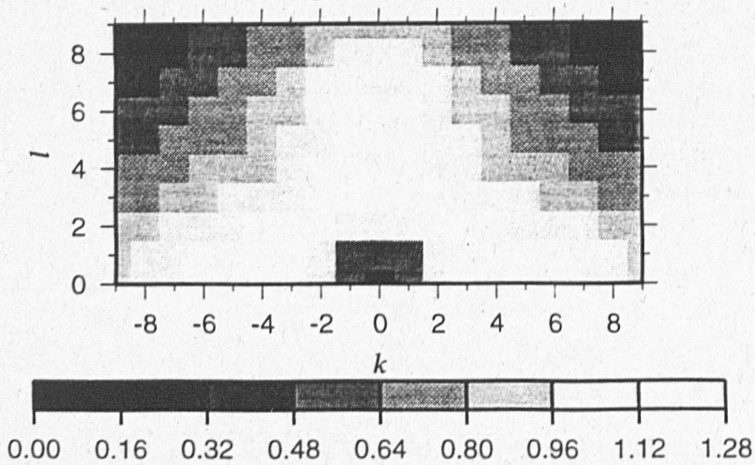

Average = 0.86 Maximum Value = 1.25 Minimum Value = 0.25

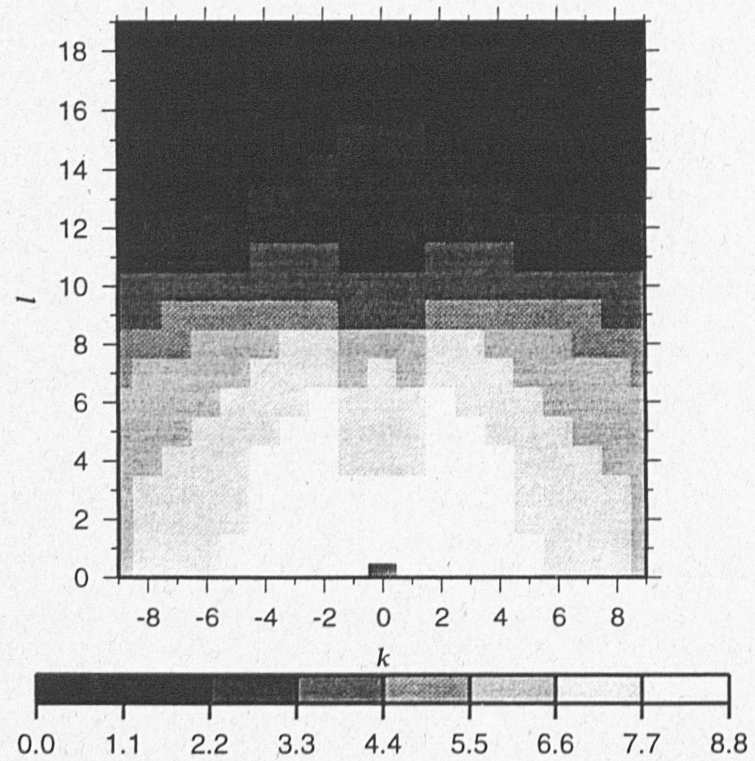

Average = 4.39 Maximum Value = 8.62 Minimum Value = 0.41

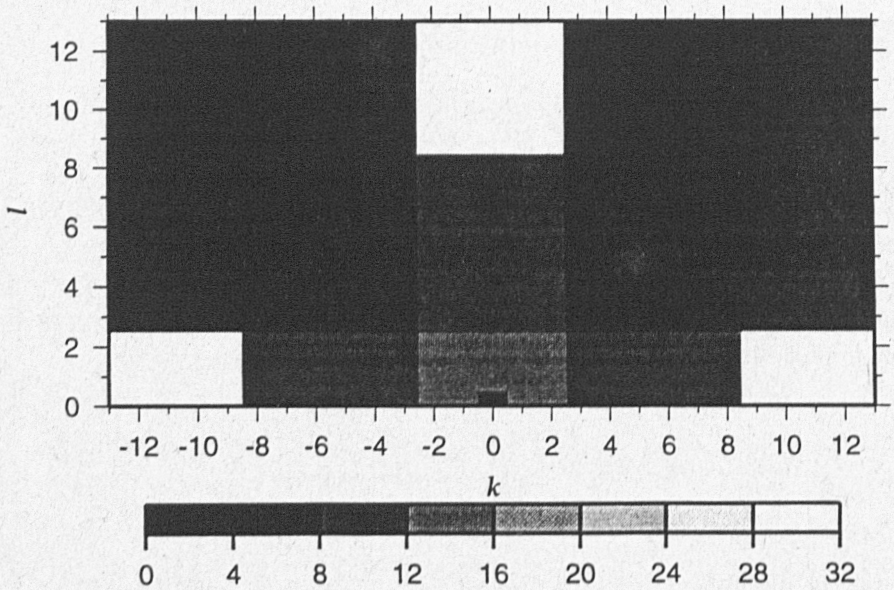

Average = 8.54 Maximum Value = 30.08 Minimum Value = 0.47

Fig. 6

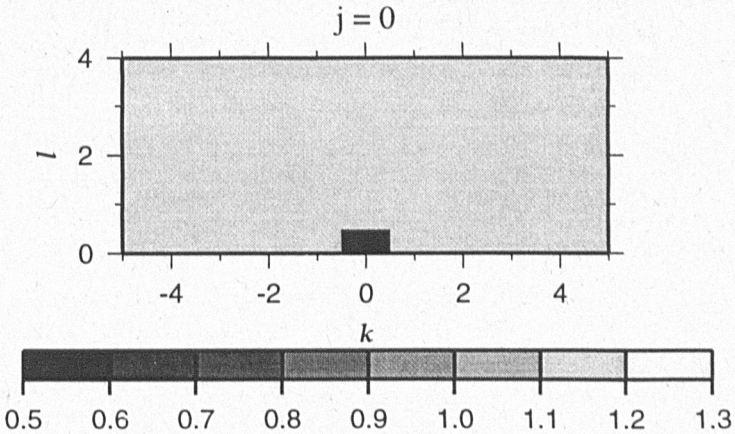

Average = 1.14 Maximum Value = 1.16 Minimum Value = 0.58

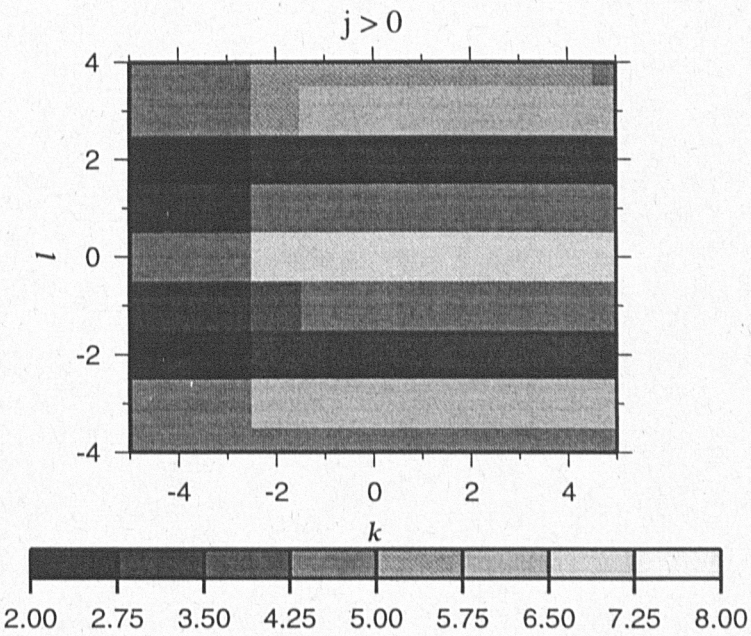

Average = 4.69 Maximum Value = 7.14 Minimum Value = 2.67

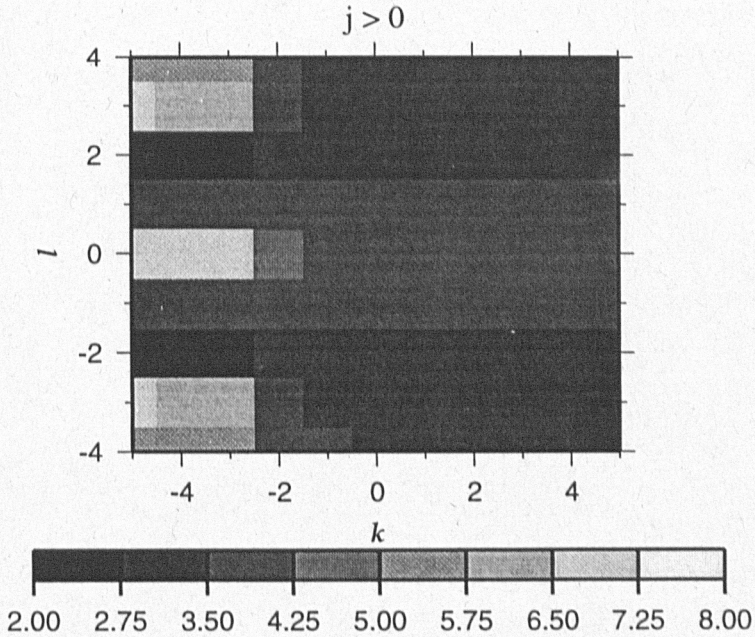

Average = 3.97 Maximum Value = 6.69 Minimum Value = 2.70